CRC-ACS TM 10075

Tow Architecture and Mechanical Properties of 3-D Woven Composites

AFOSR/AOARD Grant AOARD 09-4112

Year 1 Final Report

L. Djukic, M. Bannister and I. Herszberg

Summary

Gold and iodine contrast enhancements were applied to tows prior to weaving of multi-layer carbon fabrics in order to facilitate microCT scanning. Glass-fibre tows were also placed into multi-layer carbon fabrics in order to provide density difference, resulting in contrast with the untreated carbon. These methods allow visualisation of the tows within the weave.

Following CT scanning, the resultant images were processed using AMIRA, then converted into finite element models using two different procedures. The first was using CATIA to further process and smooth the volume, followed by paver meshing in ANSYS Workbench, resulting in an irregular mesh which conformed to all tow boundaries within the fabric. The second was automated voxel modelling using a Python script written as part of this research program, resulting in an approximate yet regular mesh.

June 2010

Acknowledgements

This work was supported by AFOSR/AOARD grant AOARD 09-4112, *Tow architecture and mechanical properties of 3-D woven composites,* program manager Dr. Kumar Jata. This support is gratefully acknowledged.

The assistance of Dr Carl Power from the University of New South Wales, School of Medicine, in running the Siemens Inveon is acknowledged. Inspections using the Skyscan 1072 were performed at the University of New South Wales, Electron Microscope Unit.

The Authors gratefully acknowledge Michael Marelli from the Cooperative Research Centre for Advanced Composite Structures, Sydney, for his assistance in the preparation of specimens.

Table of Contents

List of Tables

List of Figures

1 Introduction

This is a report summarising the first year of work of research performed under AFOSR/AOARD Grant AOARD 09-4112 “Tow architecture and mechanical properties of 3-D woven composites”. Composite structures manufactured from 3-D woven preforms have improved through-thickness properties compared to those manufactured from unidirectional lamina, however, their in-plane properties may be reduced [1].

This research program involves characterisation of 3-D woven carbon composites, and is divided into two components. The first is further advancement of the microCT contrast enhancement methods developed under AFOSR/AOARD Grant AOARD-07-4003 “Enhancement of Tow Visualisation in 3-D Woven Composites” [2-4]. The second is finite element modelling of woven fabrics, with geometry taken directly from the microCT imagesets.

In order to model the mechanical properties of such structures it is essential to determine the tow architecture and in particular any local deformations due to the interaction of adjacent tows during compaction [5]. A number of approaches to modelling of woven structures have been used previously, an in-depth summary of which was provided by Bogdanovich [6]. One of these methods involves modelling of individual tows and the matrix using idealised geometries with dimensions found using statistical methods; however, these methods can neglect details of consolidated tow geometries, resulting in inaccurate predictions. In-situ tow visualisation has been achieved in the past by means of a labour intensive serial sectioning technique [7]. Images of the specimen edge are obtained using an Optical or Scanning Electron Microscope. Progressive removal of a small depth of edge material allows the production of a series of section images which can be used to construct tow volume visualisations and finite element models.

A more efficient method by which to capture in-situ tow architectures is to use microCT scanning. The infused tows (or yarns) in woven carbon/epoxy and carbon/polyester composites are of similar density to the surrounding resin. This leads to difficulties when examining such composites using X-ray microCT scanning. The locations of tow interfaces are often difficult to determine, particularly if the tows are co-aligned. The difficulties associated with visualisation were previously treated using contrast enhancement procedures applied to individual tows prior to weaving of 2-D plain weave fabrics [2-4]. The best methods were deemed to be the use of gold to coat the exterior of tows, iodine contrast agents to coat tows throughout their volume, and use of glass tows to provide contrast against the carbon tows.

The first objective of further advancing the microCT visualisation methods was addressed through the development weaving apparatus specifically for manufacture of carbon composites with the aforementioned contrast enhancements, and is discussed in this report. Further details can be found in the project interim reports [8-10].

The second objective of finite element modelling using in-situ tow architectures, involved development of methods by which the results of microCT scans can be converted into 3-D volumes for subsequent characterisation, which was discussed in Interim Report 2 [9] and a conference paper [11]. Further discussion is provided on this point in the current report, including the use of automated voxel meshing to reduce the overall modelling time.

2 Weaving loom design, modifications and manufacture

Most commercially available table looms are designed for weaving common textile yarns such as wool and cotton. The difference in flexibility, extensibility, and strength between these common yarns and carbon yarns presents a problem when performing weaving. These problems can be accounted for through modifications to the weaving process and apparatus. An Ashford Table Loom (8 Shaft, 610 mm) was purchased for this purpose. This was placed on a table as shown in the schematic view in Figure 1. The following loom modifications were required to allow carbon fabric weaving:

1. Let-off: A specially built tensioning rack is used in the place of the warp beam supplied by the manufacturer. The let-off is therefore external to the loom.
2. Take-up: The take-up roller supplied by the manufacturer is not used, but rather a tie-off beam which is placed in front of the fabric, ahead of the loom.
3. Beat-up control: Modification used to control compaction of the weft yarns during insertion.

Each of these three modifications is elaborated upon in this section.

2.1 Let-off

In the loom supplied by the manufacturer, the warp tows are attached to the warp beam during setup and tensioned using a roller and ratchet. When tensioning using this method, the slack generated due to differences in yarn length and alignment between the let-off and the take-up is removed in common yarns; however, the aforementioned differences in flexibility and extensibility of carbon tows prevent this method from being successful in the manufacture of carbon fabrics. Hence, a different method of ensuring uniform warp yarn tension is required.

This is done using a tensioning rack, a schematic view of which is shown in Figure 1(a). The yarns are oriented to the vertical direction within tensioning rack, at which a point weights are attached in order to provide uniform warp tension. A series of rollers is used to steer the yarns into an appropriate alignment prior to entering the heddles. Rollers are spaced, such that the yarns do not touch prior to entering the heddles.

Long setup times are required between consecutively manufactured fabrics if a complete setup is required. In order to minimise this downtime a series of bobbins were spooled and placed at the bottom of the tensioning rack. These acted as creels and provided a continuous stream of yarn to the loom. Without this, the effective length of fabric produced in a single is limited to be the vertical length of the tensioning rack. This is particularly useful when producing the same fabric configuration, and adding or changing the contrast enhanced tows.

2.2 Weights

The weights used for yarn tensioning were "size 3" (19 g) lead fishing sinkers. These were partially split along approximately half of their diameter, in order to allow insertion of a 2.5 mm nylon venetian blind cord. The split sinker was then closed, forming a loop. The weights were wrapped around the yarns to form loops, as shown in Figure 2; hence they are easily removed and relocated. The resultant friction is sufficient to transfer the tensioning load. The horizontal orange cords shown in the image are used to separate tows and prevent tangling.

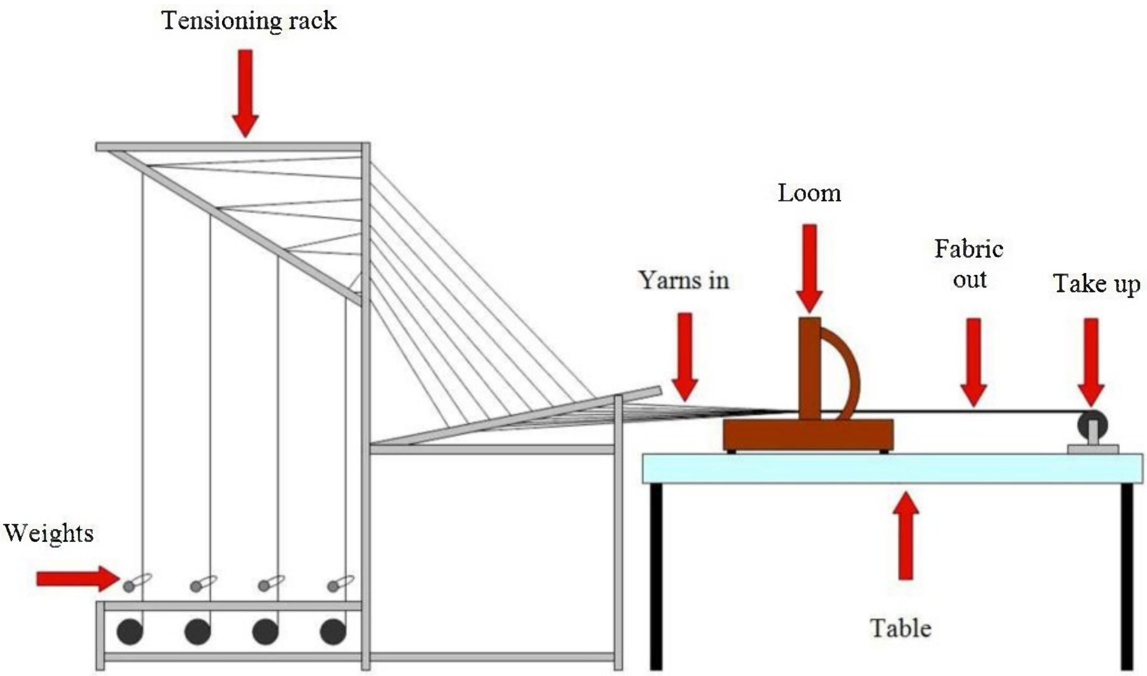

(a)

(b)

Figure 1: Loom with modifications; (a) schematic view; (b) image of setup.

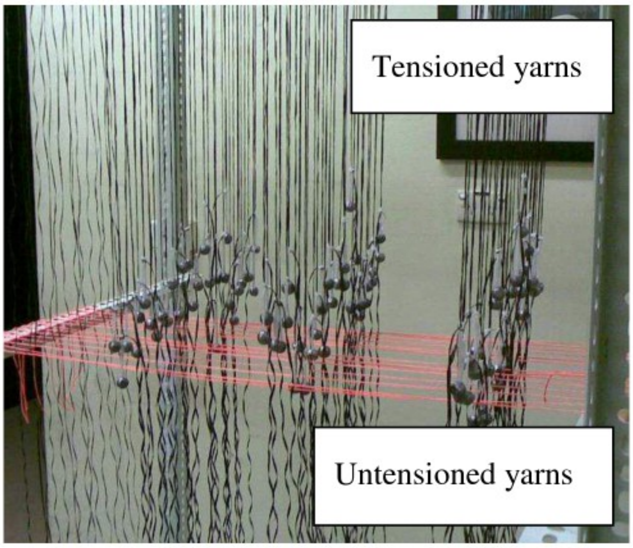

Figure 2: Weights used to tension tows.

2.3 Tensioning rack rollers and loom shafts

The first tow realignment, after tensioning by the weights, utilises individual rollers for each yarn as shown in Figure 3(a), and is referred to as "inclined individual rollers". Each line of rollers holds yarns belonging to two shafts; hence there are four lines of rollers in total. These rollers have the function of removing relative slack between yarns prior to entering the rollers that follow.

The second tow realignment is a series of long rollers with ball bearings on either side, as shown in Figure 3(b), and these are referred to as "vertical bearing rollers". Yarns belonging to each shaft are assigned to their own roller; hence, there are eight rollers in total. The third series of rollers are similar to the second, and are referred to as "inclined bearing rollers" (Figure 3(c)). No rollers are present between those shown in Figure 3(c) and the shafts shown in Figure 3(d).

2.4 Take-up

The take-up supplied by the loom manufacturer operates through gradual wrapping of the yarns and completed fabric around a roller. The roller is held in position using a ratchet. This is once again designed for use with conventional yarns. Whilst this component may be used for more flexible carbon fabrics such as plain, twill, and satin weaves, it is unsuitable for multi-layer fabrics and preforms because of their high stiffness and the potential for damage by being bent in a relatively small radius.

Instead, the yarns are tied to a beam clamped to the surface of the table. The "tie-off" beam is displaced vertically downward from the breast beam, in order to facilitate weaving. The clamping position can be moved gradually in order to allow longer fabrics to be manufactured. Another possibility which will be considered in the future is moving the roller off the loom, to the position of the clamped beam; this will allow the fabric length to be incremented without moving the tie-off beam.

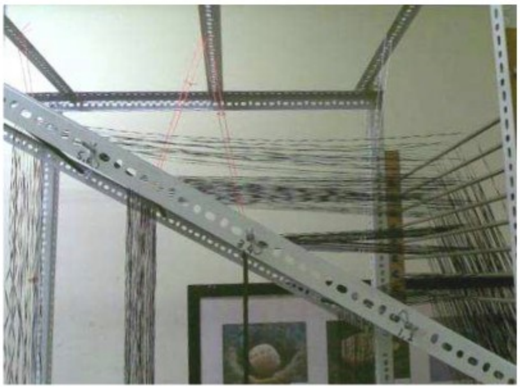

(a) *(b)*

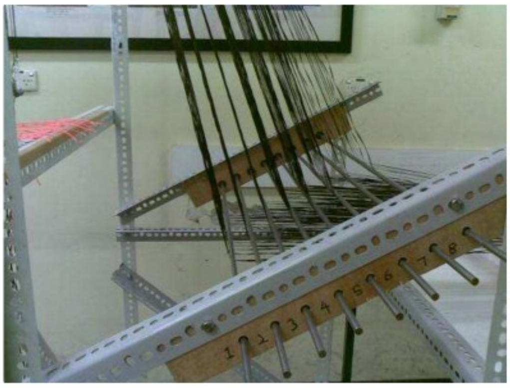

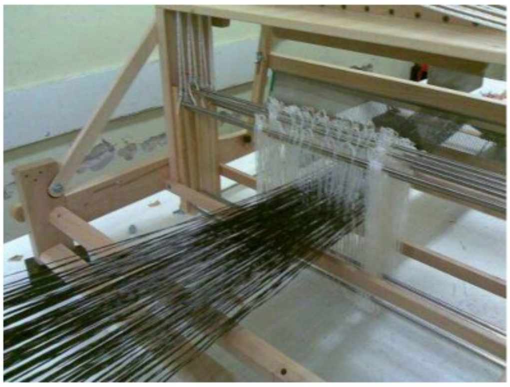

(c) *(d)*

Figure 3: Rollers and shafts; (a) inclined individual rollers; (b) vertical bearing rollers; (c) inclined bearing rollers; (d) shafts.

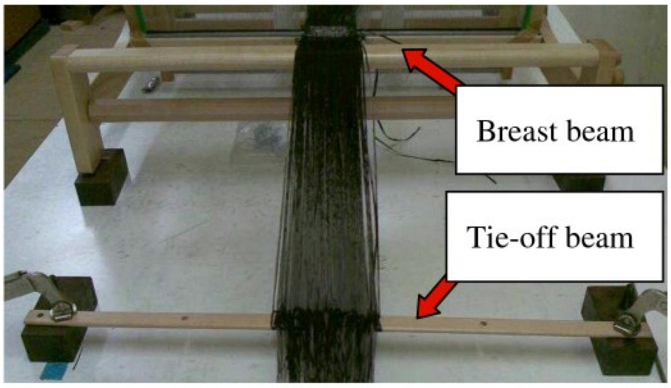

Figure 4: Modified take-up.

2.5 Beat-up control

To ensure uniform compaction of the weft during weaving, a beat-up control has been placed between the breast beam and the reed. It comprises a long threaded rod and handle that is incremented by the desired weft tow thickness at each insertion. Contact between the rod and reed prevents over-compaction of the weft tows as the result of differences in beat-up force.

Figure 5: Beat-up control.

3 MicroCT scanner specifications

The University of New South Wales has two microCT scanners. Both were used during this study. The first is the Skyscan 1072, which was used previously for developing the contrast enhancement methods and this is shown in Figure 6(a). This unit has a maximum voltage and current of 80 kV and 100 μA, respectively. This scanner is designed for inspecting small samples and has a maximum resolution of approximately 8 μm. It has an internal X-ray CCD camera with a resolution of 1024x1024 pixels. During scanning the source and detector are stationary, and the sample rotates.

The second is a Siemens Inveon CT scanner, as pictured in Figure 6(b). This also has a maximum source voltage and current of 80 kV and 100 μA, respectively. The scanner is designed for scanning small live animals such as mice, and has a maximum resolution of approximately 15 μm. The internal X-ray CCD camera has adjustable resolution, the maximum being 2048x3096 pixels. During scanning the source and detector rotate, whilst the sample is stationary.

(a) *(b)*

Figure 6: MicroCT scanners at UNSW; (a) Skyscan 1072; (b) Siemens Inveon.

4 Specimen manufacture

Three contrast enhancement procedures are considered in this study. These include coating of the outside of the tows in gold using a sputter coater, coating of the entire tow (exterior and interior) with an iodine contrast agent, and the use of glass tows to contrast against the carbon tows.

Gold coatings with a nominal thickness of 50 nm were placed on the surface of tows using an EmiTech 550X gold sputter coater. Each run of the coater results in a 25 nm coating, and so each tow required two coatings on either side.

The tows to be coated with iodine were placed into a solution of Isovue®370 and distilled water in the ratio of 1:5. Upon soaking for approximately 1 minute, the tows were removed from the solution and placed in an oven to enforce rapid evaporation. Once dried, the tows were observed to stiffen significantly. In order to re-establish their initial flexibility, the tows used in the plain woven fabrics were wrapped around a bar with radius of 15 mm, which proved partially effective. The method of increasing the flexibility was improved when weaving the multi-layer fabrics, by rolling the yarn through 360° on a 5 mm diameter venetian blind wheel. There was no relative motion (rubbing) between the yarn and the wheel.

The use of glass within a carbon fabric was undertaken without physical coating, since the method relies on difference in the density relative to the carbon tows. There was, however, the consideration of having a similar cross section between both the carbon and glass yarns. In order to establish this, large glass tows were obtained and carefully split by, such that the cross sections were visually similar by eye.

4.1 Plain woven fabrics

Plain woven fabrics were manufactured using 3K T300 tows that had been treated with gold and iodine. The iodine tows were used as the warp, whilst the gold tows were added as the weft. Three fabrics of this type were manufactured and placed centrally within different laminates of $[0/90]_8$ configuration. Hexcel 282 plain weave carbon fabric (3K tows, 197 gsm) was used to make up the remainder of the laminate. The first laminate (PGI1) was consolidated with polyester resin using vacuum bag resin infusion (VBRI) at room temperature.

The second laminate (PGI2) was consolidated with Hexcel M36 epoxy resin using Resin Film Infusion (RFI) in an autoclave at 177˚C and 610 kPa.

The third (PGI3) was infused in a similar fashion to the second (PGI2); however, the treated ply was placed in contact with the tool surface on the outside of the laminate rather than at the centre.

4.2 Multi-layer fabrics

Multi-layer fabrics of the configuration shown in Figure 7 were manufactured using the aforementioned loom. The warp is divided into three layers, composed of 6K T300 carbon tows, and is oriented out of the page in Figure 7 (a)). There are four weft layers, composed of 6K T300, oriented across Figure 7 (b). Through-thickness 3K T300 tows are present between each pair of 6K warp tows.

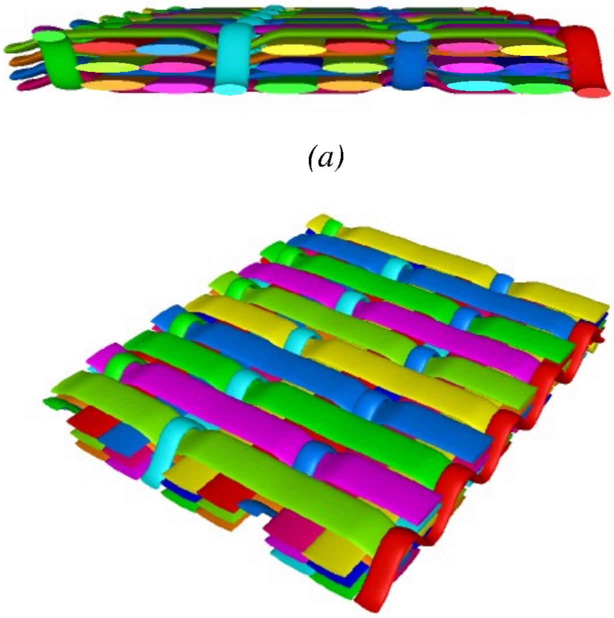

(a)

(b)

Figure 7: Schematic view of multi-layer fabric configuration used throughout testing. Image generated using TexGen[1].

In the case of the warp and through-thickness tows, the contrast enhancement techniques were used in the fabric by replacing segments of the uncoated carbon tows already present on the loom with contrast enhanced tows. This was done by gluing the ends of the contrast enhanced tows into position on the loom, then cutting the existing uncoated tow. In the case of the weft tows, the contrast enhanced tows replaced the uncoated tows present on the shuttle.

4.3 Test matrix

Samples with a P as the first letter in their designation contain a contrast enhanced plain woven fabric, whereas an M indicates multi-layer fabric. The letters directly following this can be one of GI – gold/iodine; GF – glass-fibre tows; I – iodine; G – gold. The number in the designation is the sample number fitting this description.

A source voltage and current of 80 kV and 100 μA was used during scanning, irrespective of the scanner used for the inspection. A list of the differing scan parameters and dimensions is given in Table 1. The coated tow direction is listed in brackets under the sample designation.

Note the variation in the exposure times for the newly added samples in the test matrix shown in Table 1. Where 1.9 seconds was used on the Skyscan 1072 previously, it has been increased, the longest time being 2.7 seconds in the case of MGFGI1. This increase was necessary due to the larger amount of high density material within the laminates, which prevented sufficient penetration from the source to the detector.

[1] TexGen 3.3.0, *The University of Nottingham.*

Table 1: Sample dimensions and scan parameters.

Sample	Scanner	Width (mm)	Thickness (mm)	Exposure (s)	Pixel (μm)	Total angle (°)	Angular increment (°)
PGI1	Skyscan	3.96	1.91	1.9	6.5	180	0.225
PGI2	Skyscan	5.08	1.95	1.9	6.8	180	0.225
PGI3	Skyscan	7.15	2.04	1.9	8.3	180	0.225
MGF1	Siemens	15.58	2.11	6.0	10-15	192	1.0
MGF2	Skyscan	6.55	3.80	1.9	8.8	180	0.225
MGF3	Skyscan	5.94	3.33	1.9	7.6	180	0.225
MI1	Skyscan	5.54	2.40	1.9	7.6	180	0.225
MG1	Skyscan	5.30	2.56	1.9	7.6	180	0.225
MG2	Skyscan	6.13	2.12	1.9	8.5	180	0.225
MG3	Skyscan	6.35	2.06	1.9	9.1	180	0.225
MGFI1	Skyscan	6.74	3.07	2.2	9.1	180	0.225
MGFGI1	Skyscan	6.82	3.21	2.7	9.1	180	0.225

5 Results

5.1 Pre-microCT scan inspection

Images of the dry preforms prior to infusion are oriented such that the weft direction is vertical, whilst the warp direction is horizontal. The dry multi-layer glass fabrics are shown in Figure 8. The glass weft tows pictured centrally in Figure 8(a) are present throughout the entire thickness of the laminate (i.e. the fabric looks similar when viewed from the opposite side). Visually, the glass weft tows look similar to the regular carbon tows.

The glass warps shown in Figure 8(b) are of slightly different appearance to the surrounding carbon. The through-thickness tow is marked by the dashed red line, and its presence has significantly distorted the fabric in comparison to the regular 3K carbon through-thickness tows. This is the result of the glass tow having a stiffer cross-section, and this issue may be treated through more careful selection of glass-fibre tow.

The single centrally located glass warp tow is visible on either side of the image; however, since it is present within the centrally located warp layer, it is hidden at the centre of the image. It is marked with a dashed white line since it is not visible in the image. There is no apparent distortion of the fabric surface.

Nearest the bottom of the image, there are three glass warp tows stacked in consecutive warp layers on top of one another. This has had a slight effect on the top surface of the fabric; the through-thickness tows appear more spread out in the vertical direction than in the neighbouring regions of the fabric, indicating greater spreading of the warp tows in general in this area. This may be due to the glass warp tows being slightly larger than the carbon, since they were produced by splitting larger glass tows, through visual inspection.

A general comment on the appearance of the fabric is that there was significant glass fibre breakage during weaving, which can be seen around the fabric in Figure 8(b).

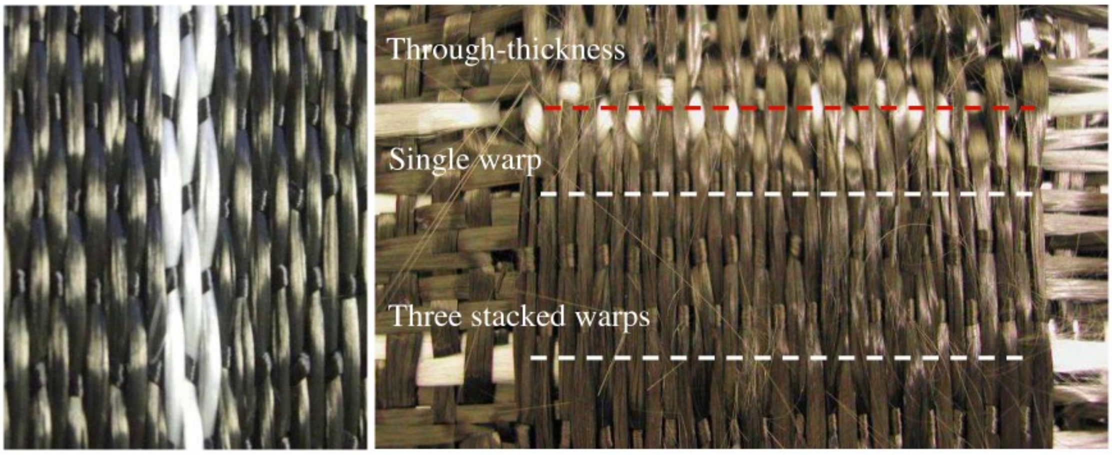

(a) *(b)*

Figure 8: Dry multi-layer fabrics containing glass; (a) weft direction (MGF1); (b) warp direction (MGF2).

An infused multi-layer fabric containing gold and iodine coated warps and through-thickness yarns is show in Figure 9. The gold through-thickness tow is the only visible tow in the list, as indicated by the red dashed line.

The locations of all other coated yarns are marked with dashed white lines. The iodine coated through-thickness tow is indistinguishable from the other uncoated carbon tows; however, it is visible in the image. The gold and iodine warp tows are located at the centre of the laminate, hence they are not visible, aside from a small portion of the gold coated tow present outside the woven section at the top left of the image.

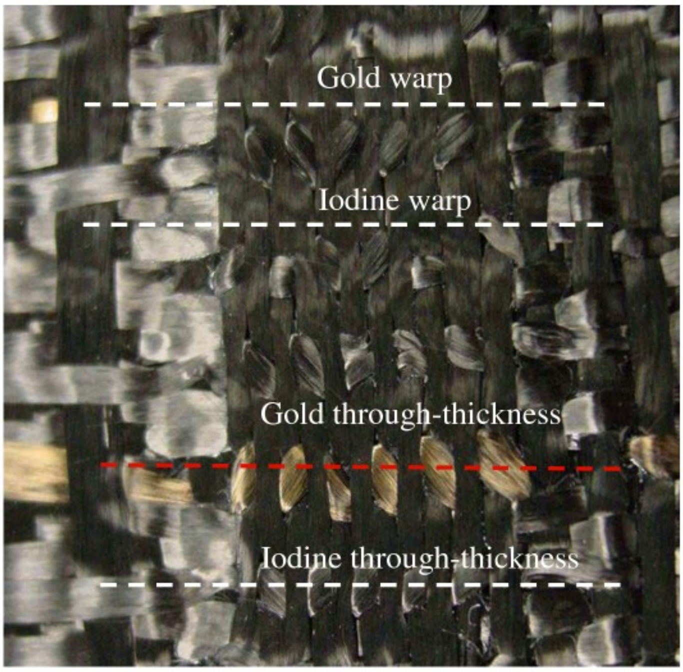

Figure 9: Infused multilayer carbon fabric containing gold and iodine coated tows.

5.2 MicroCT scan results

The cross-sectional images derived from the scans were reconstructed using either NRECON[1] (Skyscan, Belgium) or Siemens Inveon software. Images generated with NRECON are oriented such that the lower edge of the sample is that which was in contact with the tool surface during infusion.

In selected instances, 3-D volume renderings are presented alongside the cross-sectional images, and were generated using two different programs. The first program is 3-D CREATOR[2] (Skyscan), which is capable of generating volume representations very quickly, but does not have the versatility to account for problems brought about by events such as artifacts. The second is AMIRA[3] coupled with CATIA[4], and can be used to generate more accurate volume representations; however, rendering takes a significantly longer time.

5.2.1 PGI1 – Plain weave with gold and iodine coated tows

The gold and iodine coated tows are clearly present within the treated fabric shown in Figure 10. The gold can be seen as thin bands surrounding the tows, whilst the iodine is present throughout the treated tow. Tow deformations which occurred during compaction are visible. The void fraction of this sample was not significantly different from the general 0.4% found in composites.

[1] NRECON, *Skyscan.*
[2] 3-D CREATOR, *Skyscan.*
[3] AMIRA® 4.1.1, *Visage Imaging.*
[4] CATIA® V5R18, *Dassault Systemes.*

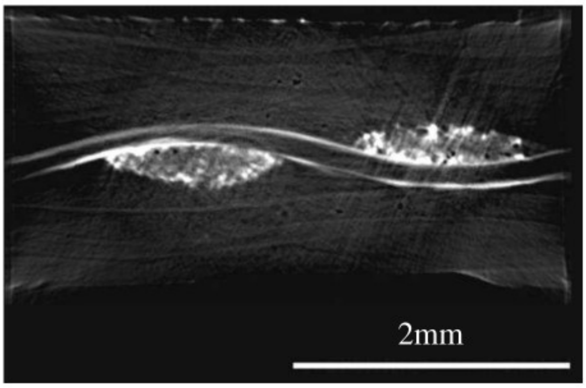

Figure 10: Cross-sectional image of laminate with gold and iodine coated plain woven ply (PGI1) consolidated using VBRI.

5.2.2 PGI2 – Plain weave with gold and iodine coated tows

The contrast generated in PGI2, shown in Figure 11(a), is very similar to PGI1. However, the higher pressure of 610 kPa used during infusion has had a significant effect on the deformation of the tows, in comparison to the previous infusion done under vacuum pressure, which can be seen through comparison of Figure 11(a) and Figure 10. Note that PGI2 is the laminate from which the finite element model discussed in Interim Report 2 [9] was generated.

The 3-D volume rendering in Figure 11(b) was generated using AMIRA and CATIA. This has allowed separate visualisation of the tows, along with cleaning of the volume from events such as artifacts, both of which would not have been possible using 3-D CREATOR[3].

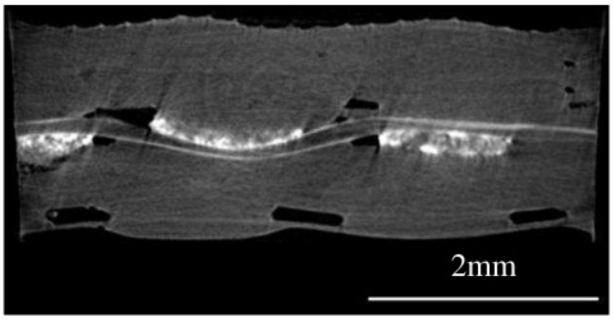

(a)

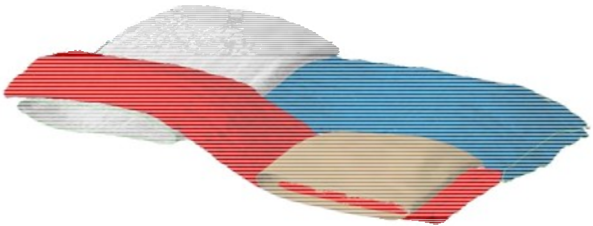

(b)

Figure 11: Laminate with gold and iodine coated plain woven ply (PGI2) consolidated using RFI; (a) Cross-sectional image; (b) 3-D volume rendering.

5.2.3 PGI3 – Plain weave with gold and iodine coated tows

A single iodine coated tow is oriented across both Figure 12(a) and (b), whereas four gold coated tows can be seen within the image and are oriented out of the page. Considerable distortion of the gold coated tows can be seen at the iodine coated tow interfaces and the untreated regions of the laminate. As expected, the locations in which the tows were in contact with the tool surface during consolidation are flat.

The void content of the sample was measured at 4.6%, which is high in comparison to the more readily accepted void fraction of 0.4%. The higher void fractions were found in the untreated composite layers, adjacent to the tows that were treated with iodine, as shown in Figure 12(a). In the locations where only gold tows were present, such as the situation shown in Figure 12(b), the void fraction was much closer to the more readily accepted value, indicating the iodine coating promotes the higher void content.

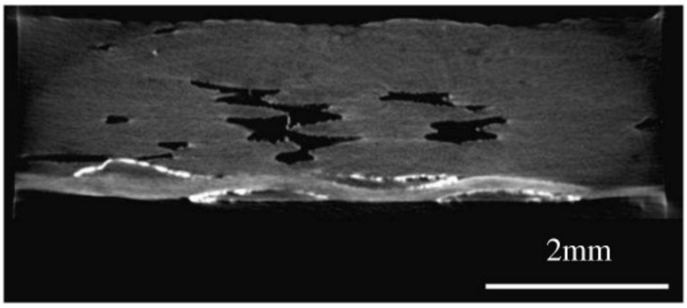

(a)

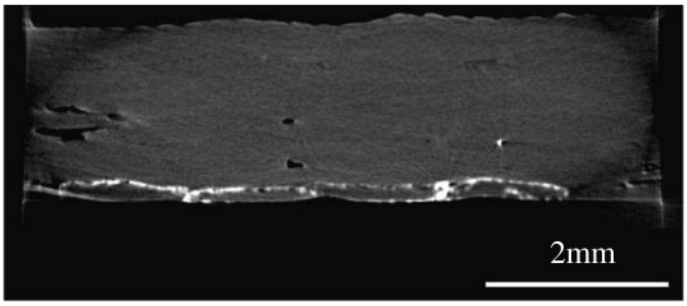

(b)

Figure 12: Laminate with gold and iodine coated plain woven ply on surface (PGI3) consolidated using RFI; (a) high void fraction area; (b) low void fraction area.

5.2.4 MGF1 – Glass weft in multi-layer fabric

The results of the scan of MGF1 are shown in Figure 13. The location of the green cross-hair is consistent in all three images. This visualisation was generated using the Siemens Inveon CT scanner. The untreated through-thickness carbon tows cause localised compressions in the transverse directions of the glass tows (perpendicular to fibre axis), which is visible in Figure 13(a). Away from the through-thickness carbon tows, the yarns are more spread out. The regions in which the glass tows are observed to come into contact with one another appear to have slightly brighter appearance; this may be the result of an average density increase as a result of a locally high fibre volume fraction.

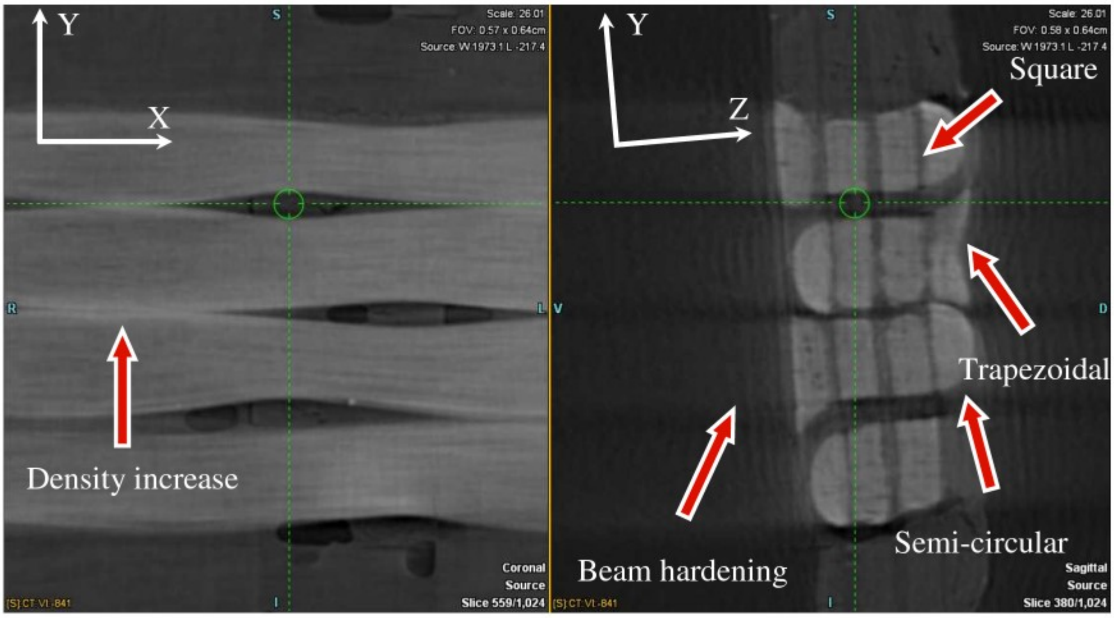

(a) *(b)*

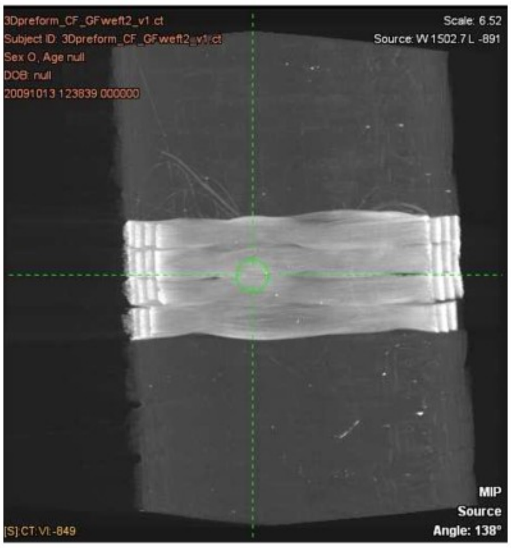

(c)

Figure 13: Glass tow weft in multi-layer fabric (MGF1); (a) XY-plane; (b) YZ-plane; (c) 3-D reconstruction perspective view.

There are visible differences in the tow deformations at various points in the weft as shown in Figure 13(b). The darkened regions which interleave the glass tows in the Z-direction are carbon warp tows. The darkened regions which space the glass tows in the Y-direction are the result of a single through-thickness tow passing through the cross-section. The centrally located glass weft tows appear approximately square. The weft tows that are on the outer surface of the fabric and encapsulated by the through-thickness tow appear semi-circular as indicated in the image, whilst those on the outer surface that are not encapsulated appear almost trapezoidal.

The series of staggered white lines of approximately vertical orientation on either side of the fabric shown in Figure 13(b) may be beam hardening artifacts. The artifact is not continuous, as was the case in the previous study involving glass tows, since an angular increment of 1° was used during image acquisition, rather than 0.225°. Hence, the artifact appears more discrete. The deformations present in the glass tows are shown throughout the volume in Figure 13(c).

5.2.5 MGF2 – Single through-thickness glass tow in multi-layer fabric

A single carbon through-thickness tow was replaced with a glass tow, and woven into the multi-layer fabric, as can be seen in Figure 14 (also pictured optically in Figure 8(b)). The regular carbon tows and resin surrounding the glass tow appear slightly brighter than the rest of the composite as a result of beam hardening artifact. In addition, small regions of higher density can be seen throughout the composite; these are small bundles of glass fibres which are present in the remainder of the fabric due to fraying of the tow during weaving.

The glass tow spans a considerable distance in the weft direction as shown in Figure 14(b). This behaviour differs from the regular carbon tows, which are of predominantly vertical orientation. This difference is a result of greater stiffness in the glass tows due to the effect of tow sizing and slightly greater cross-sectional dimensions than the carbon tows.

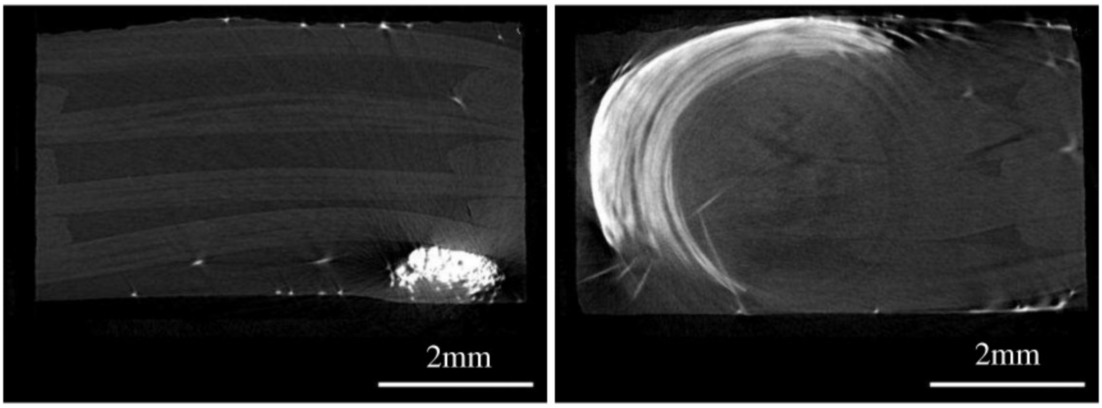

(a) *(b)*

Figure 14: Glass through- thickness tow in multi-layer fabric (MGF2); (a) glass tow at fabric exterior interface; (b) glass tow spanning composite weft direction.

5.2.6 MGF3 – Single warp glass tow in multi-layer fabric

A single glass warp is shown in Figure 15 and is oriented out of the page. The centrally located portion of the warp layer, indicated by the red ellipse, is made up of the glass tow and an untreated 6K carbon tow. The glass tow is the larger out of the two. In addition, the central warp layer is of greater thickness than those above and below, which is the result of the glass tow having either a larger cross-section, or a lower compressibility.

The co-aligned pairs of 6K warp tows in the untreated regions both above and below the glass tow are indistinguishable from one another. This reinforces the need for the contrast enhancement to distinguish between tows in woven preform structures.

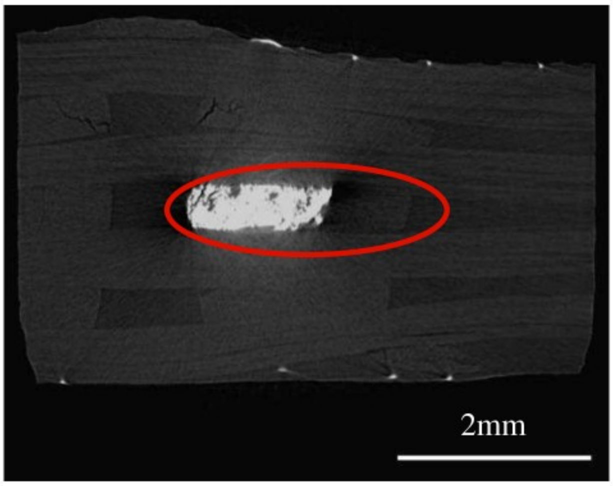

Figure 15: Single glass warp tow in multi-layer fabric (MGF3).

5.2.7 MI1 – Iodine coated wefts in multi-layer fabric

A region of multi-layer fabric containing iodine coated tows is shown in Figure 16. The two tows shown at the bottom of the fabric in Figure 16(a) are difficult to distinguish from one another at their point of contact (red ellipse); the location of the interface is uncertain. Two tows of this type would be indistinguishable if placed side by side within a warp layer, in the manner pictured in Figure 15. The coated tows appear dimensionally similar to the uncoated weft tows.

A region of the fabric containing a untreated 3K carbon through-thickness tows can be seen in Figure 16(b). The through-thickness tow appears similar to the surrounding 6K tows. This is possibly a combination of the effect of beam hardening, washing off of the tow coating during infusion, and friction between tows during weft insertion and beat-up. Gaps appear between the through-thickness tows and the weft tows as a result of poor infusion. The coated weft tow located at the bottom of the fabric and encapsulated by the through-thickness tow and the first warp layer is deformed such that it is semi-circular in cross section. To the right of this tow is another tow on the bottom of the fabric, that is not encapsulated by the through-thickness tow, and this is approximately trapezoidal in cross-section. These observations of tow deformations are similar to the glass tows shown in Figure 13(b).

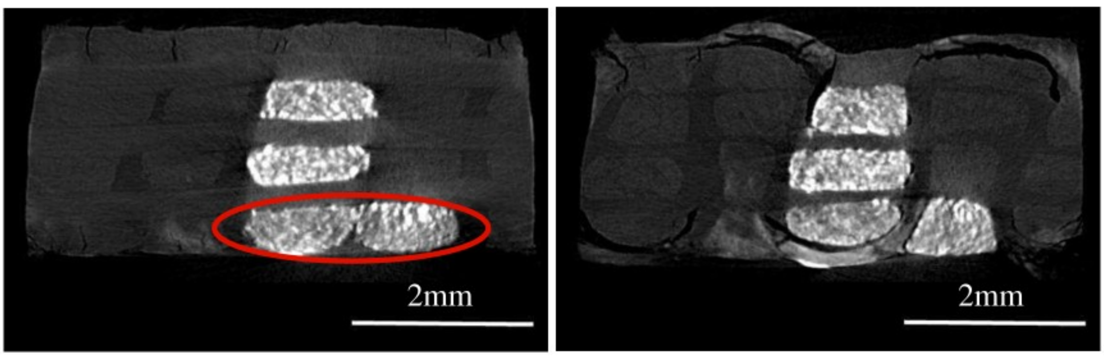

(a) *(b)*

Figure 16: Iodine coated warps in multi-layer fabric (MI1); (a) region away from through-thickness tows; (b) region containing through-thickness tows.

5.2.8 MG1 – Gold coated warps in multi-layer fabric

The gold coated tows in Figure 17(a) are shown in a region with a high density of weft tows. If these coatings were not present, it is unlikely that the tows would be distinguishable from the untreated tows directly to the right of either treated weft tow. A small line of contrast enhancement can be found in the centre of each gold coated tow in Figure 17, and this will be discussed further in Section 5. The cross-sectional shapes in Figure 17(a) differ extensively to those present in Figure 17(b).

The tow dimensions in the contrast enhanced carbon do not differ significantly from those of the surrounding untreated tows. This is similar to previous results, in which the tow dimensions were found to be statistically similar. The gold tow coating results in minimal beam hardening, and is not observed to wash off at any point, as was the case in MI1 (Figure 16(b)).

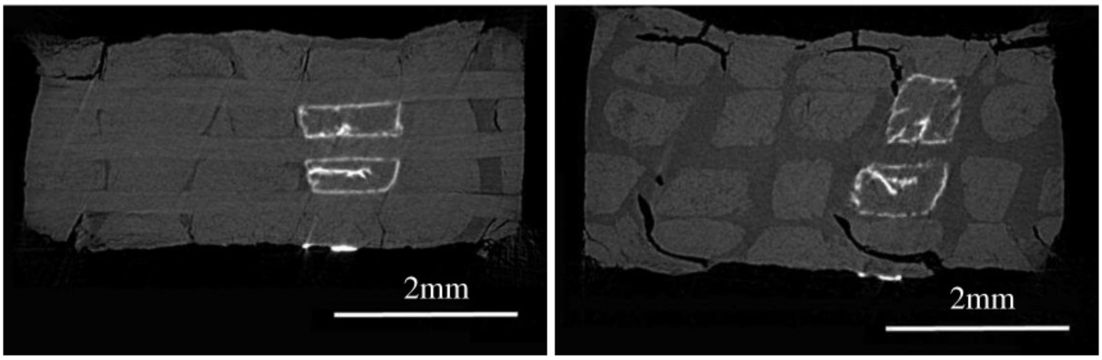

(a) *(b)*

Figure 17: Gold coated warps in multi-layer fabric (MG1); (a) region away from through-thickness tows; (a) region containing through-thickness tows.

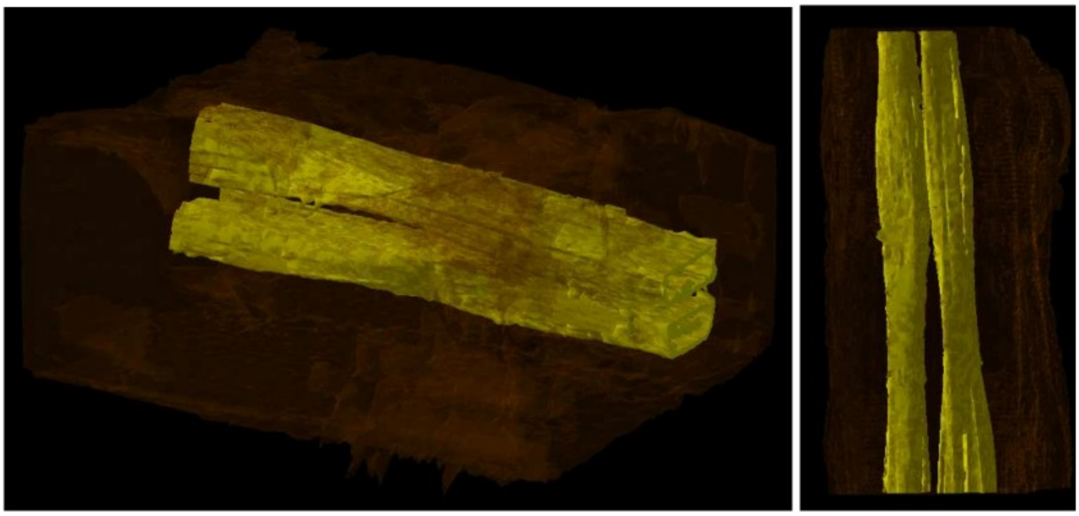

(a) *(b)*

Figure 18: 3-D reconstruction of gold coated tows in MG1; (a) perspective view; (b) side view.

The 3-D reconstructions of the gold coated tows contained within MG1 shown in Figure 18 were generated using 3-D CREATOR (Skyscan). Tow coatings are shown in yellow, whilst the outside of the composite is shown in opaque brown. Regions in which the brown appears slightly lighter indicate the presence of voids in the composite. One of the features of these 3-D reconstructions is the dimensional inconsistency between tows, which is characteristic of the multi-layer fabrics.

5.2.9 MG2 – Gold coated wefts

The results from the scan on MG2 are presented in Figure 19. The void fraction of this sample was 0.2%. This sample only contained gold contrast enhancement, and only in the weft direction. The tow interfaces are well visualised.

In all cases there is some part of the coating present inside the tows. This is the result of the tows folding in on themselves during weaving of the preform. In some cases, there is some difficulty in discriminating between the outer boundary and a fold.

Small cracks are present in the uncoated regions of the fabric either side of the coated region in Figure 19 (a). Because of their shape and location, it is likely that these formed during trimming of the panel, rather than infusion. Voids which result from the infusion process are generally wider and less sharp, and are more likely to occur outside of the tows in the resin rich areas.

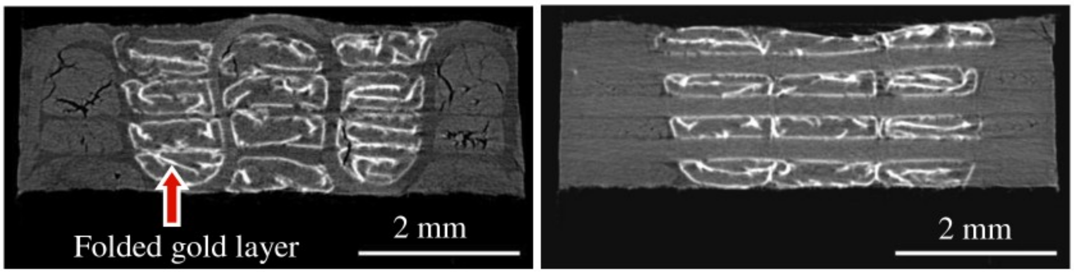

(a) *(b)*

Figure 19: Cross-sectional images of MG2; (a) Containing through-thickness tow with minimal warp; (b) No through thickness tow present but warp throughout.

5.2.10 MG3 – Gold coatings applied to all directions

The results from the scan on MG3 are presented in Figure 20. The void fraction of this sample was 0.2%. This sample contained gold contrast enhancement in the warp, weft and through-thickness tows. The tow interfaces are well visualised.

Observations related to folding of the tows are similar to those discussed in Section 4.6.9. In addition, the result of folding of the gold layers can be seen in the through-thickness tows (Figure 20 (a)) and the warp tows (Figure 20 (b)). The folds appear as long lines, which run parallel to the outer tow interfaces that are in contact with the weft tows.

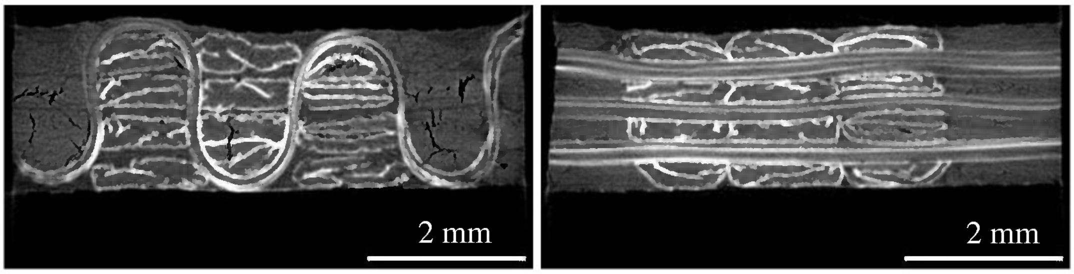

(a) *(b)*

Figure 20: Cross-sectional images of MG3; (a) Containing through-thickness tow with minimal warp; (b) No through thickness tow present but warp throughout.

5.2.11 MGFI1 – Glass-fibre and iodine coated wefts

The results from the scan on MGFI1 are presented in Figure 21. The void fraction of this sample was 0.1%. Only the weft was contrast enhanced. The coating methods are identified in the images, and are clearly distinguishable from one another.

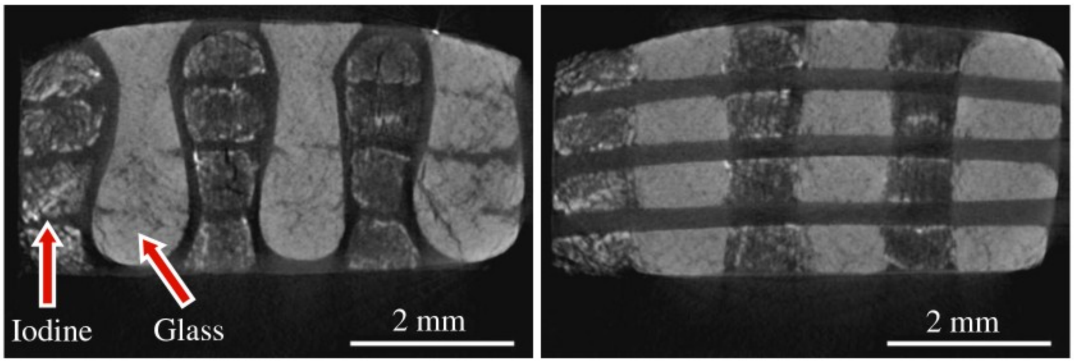

(a) *(b)*

Figure 21: Cross sectional images of MGFI1; (a) Containing through-thickness tow with minimal warp; (b) No through thickness tows present but warp throughout.

5.2.12 MGFGI1 – Glass-fibre and iodine coated wefts, gold warps

The results from the scan on MGFGI1 are presented in Figure 22. The void fraction of this sample was 0.1%. The weft tows are a combination of glass and iodine coated tows, similar to the results of MGFI1 (Figure 21). The through-thickness and warp tows are gold coated. A region containing uncoated carbon, interlaced with gold coated warp and through-thickness tows, is present at the left edge of each of the images. All contrast enhancement methods are identifiable in the images.

In Figure 22 (a), the gold layers surrounding the through-thickness tows are visible in some locations. Non-uniformities in the gold thickness render the coating ineffective in some locations, possibly as a result of poor coating or sections of the coating rubbing off during weaving. Whilst the results of the scan on MG2 (Figure 19) and MG3 (Figure 20) did reveal some non-uniformities, they did not reduce the effectiveness of the visualisation.

In Figure 22 (b), the main location in which the gold is clearly identifiable is within the folds at the tow interiors. At the gold/glass and gold/iodine tow interfaces, there is difficulty in discriminating between the gold coating and the iodine or glass tows. It is likely that the visualisations at these interfaces are a combination of the two contrast enhancements. A three dimensional volume rendering of the fabric, generated using AMIRA, is shown in Figure 23.

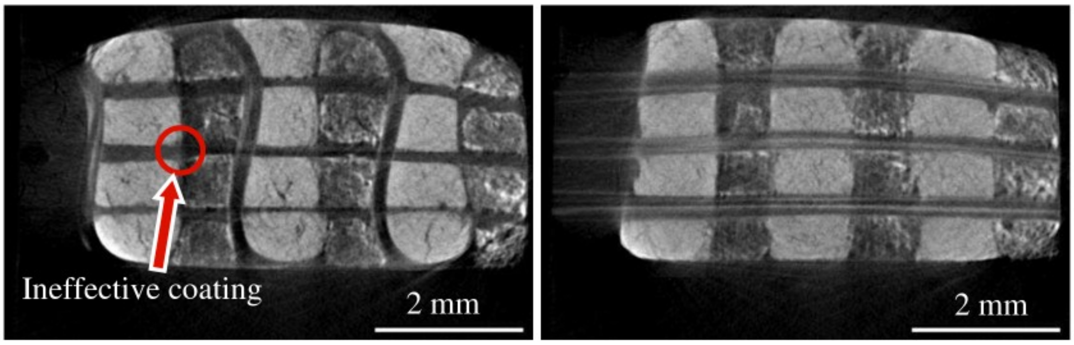

(a) (b)

Figure 22: Cross sectional images of MGFGI1; (a) Containing through-thickness tow with minimal warp; (b) No through thickness tows present but warp throughout.

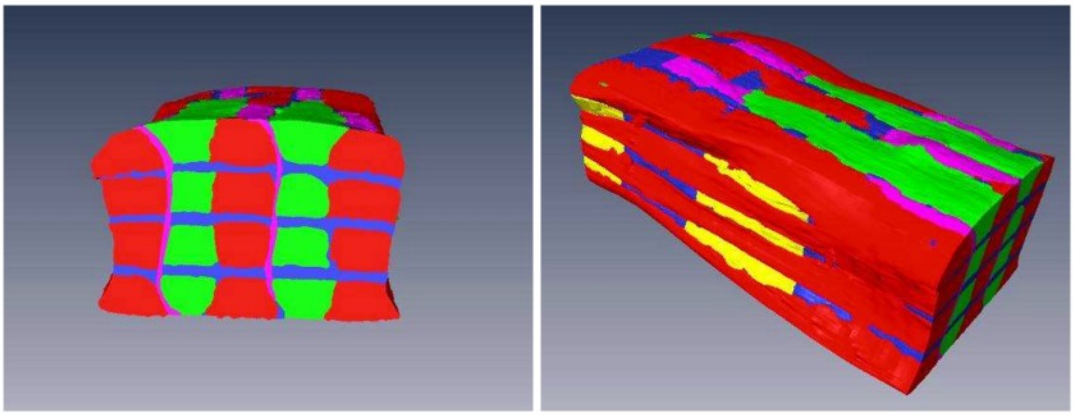

(a) (b)

Figure 23: 3-D volume rendering of MGFGI1; (a) Image 1; (2) Image 2.

6 Finite Element Modelling (FEM)

The two different finite element modelling approaches investigated in this research were conventional FEM and voxel FEM. Conventional finite element modelling is used to describe a process in which volumes of tows are processed and imported into a finite element pre-processor, where they are meshed. The pre-processor is used to apply a paving algorithm, which generates a mesh to fit a given volume, which is very irregular in this case. The conventional FEM approach was developed rapidly in order to determine the feasibility of modelling architectures from microCT scans, the success of which paved the way for additional modelling research in the form of voxel modelling.

A voxel finite element modelling approach differs to conventional finite element modelling, in that a given volume of regular finite elements is fixed, with each element being assigned properties based on the position within the volume. The key difference is that the mesh is not generated based on the volume; it is already there.

This leads to an approximation to the volume, allowing automation of the modelling process.

The two processes are illustrated diagrammatically in Figure 24. The boxes shown in green indicate that that segment of the tool development process has been completed. Those shown in yellow indicate that development is currently underway. The processes shown in red indicate areas that will be developed in the next program.

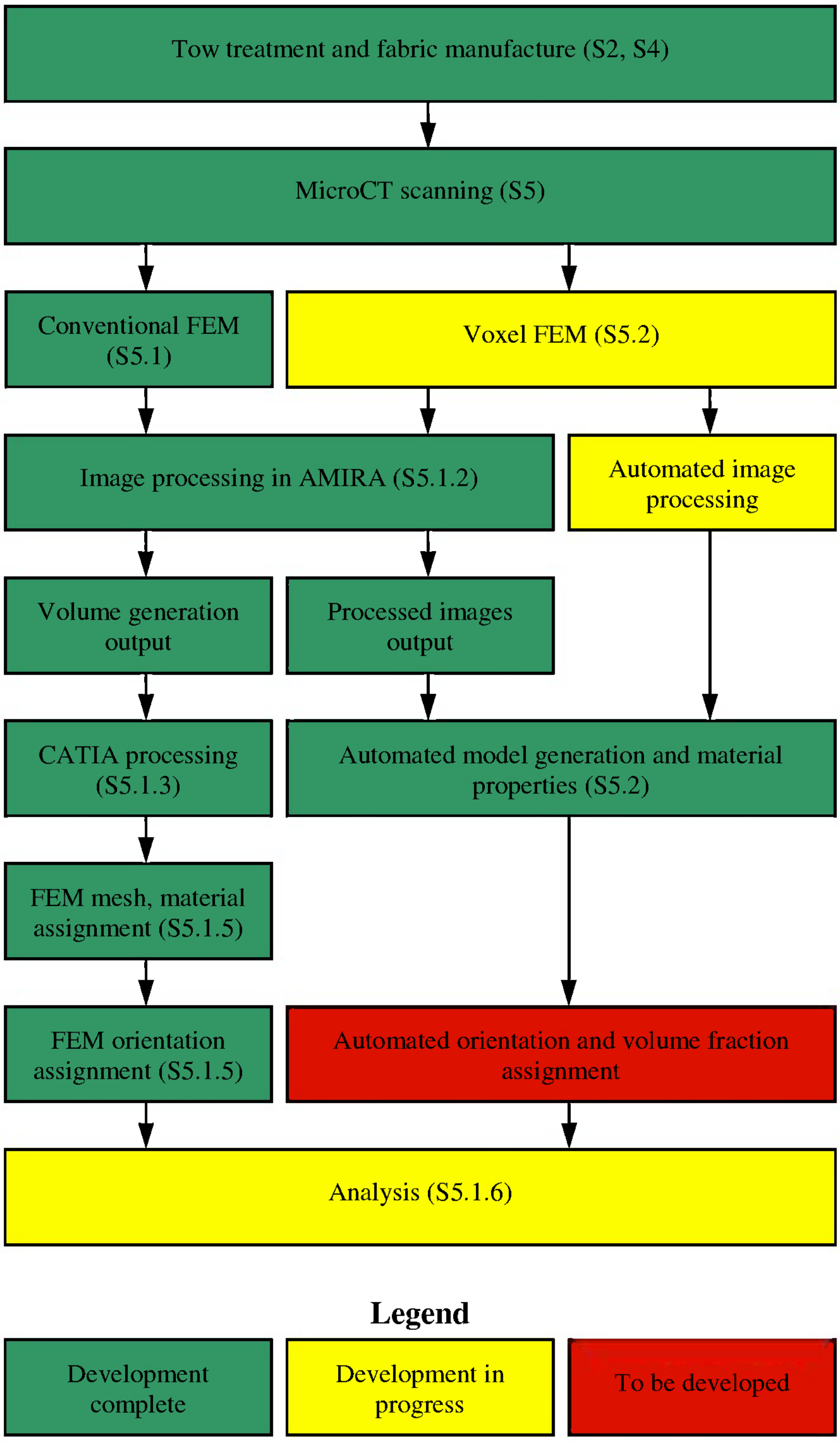

Figure 24: Finite element modelling tool development strategy.

6.1 Conventional FEM approach

6.1.1 Model generation steps

A series of steps is required in order to generate the 3-D fabric models. These must be carried out in the order that follows:

1. Sample manufacture and scanning:
    a. Contrast enhancements must be applied to the tows prior to weaving
    b. Fabric construction and composite consolidation
    c. MicroCT scanning
2. Three-dimensional volume rendering:
    a. Tow volume rendering in tomographic imaging programs (eg: AMIRA®)
    b. Conversion of volumes to STL format, readable by CATIA
    c. Importation of individual tow volumes to CATIA and fabric assembly
    d. Construction of matrix surrounding tows
    e. Generation of file format readable by finite element analysis (FEA) packages (eg: IGS)
3. Finite element modelling:
    a. Importation of IGS file into FEA package (eg: ANSYS)
    b. Volume meshing
    c. Finite element modelling steps, discussed in brief in this report.

Further detail on these steps is given in the sections that follow.

6.1.2 Volume rendering

Following cross-sectional image reconstruction, there are number of tomographic cross-sections of the sample available for inspection. The images were imported into AMIRA® 4.1 (processing can alternatively be done in Mimics®) which is a program designed specifically for postprocessing of images taken from CT scans. The images were then grayscale thresholded, and a volume was rendered as shown in Figure 25.

The volume was exported in WRL file format, from which an STL file was created using a conversion utility. This is essentially a point cloud, which describes a homogenous structure based on whether the point is visible (assigned 1) or not (assigned 0). The structure appears as a series of voxels, the length of which is based on the spacing between the cross-sectional images. Each tow within the fabric was reconstructed individually.

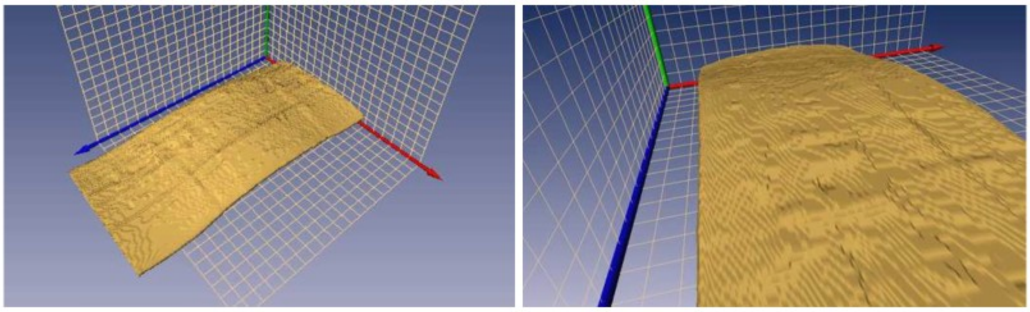

Figure 25: Reconstructed tow from AMIRA 4.1.

6.1.3 Geometric modelling within CATIA

The tow volume files were imported into CATIA V5 R18 using the Digitised Shape Editor workbench. The Shape Sculptor workbench was employed to geometrically simplify and smooth the volumes. Following this, the processed tows were reconstructed into surface models via the Quick Surface Reconstruction workbench. Finally, the tows were assembled into a woven fabric as shown in Figure 26(a), and later trimmed into a unit cell shown in Figure 26(b). The matrix was constructed around the tows after assembly of the fabric. From CATIA it is possible to generate an IGS file, which is able to be read by FEA and computer aided design (CAD) packages alike.

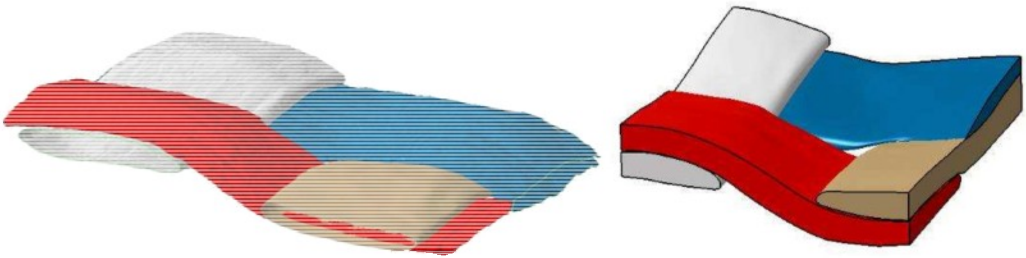

(a) *(b)*

Figure 26: Processed woven fabric as assembled within CATIA; (a) raw tow import; (b) unit cell after geometric smoothing and trimming.

It is clear from Figure 26 that the cross-sectional geometries of the tows are irregular, although they are similar in overall dimension. This is expected to cause a difference in the results obtained from finite element models of idealised tow geometries, the extent of which is yet to be assessed. Additionally, the arrangement of tows within the weave is irregular, unlike idealised models such as that shown in Figure 27.

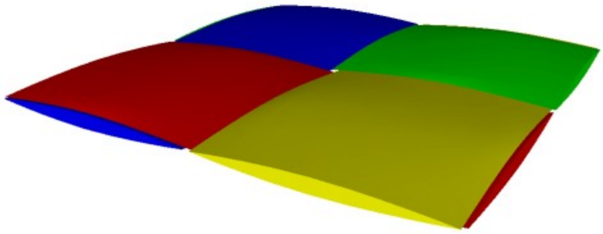

Figure 27: Idealised plain woven fabric model. Constructed using TexGen 3.3.0.

The orientation of the top and bottom surfaces of the matrix shown in Figure 28 is a reflection of the unit cell orientation relative to the laminate. This has resulted in one of the fabric edges being centrally located with large resin rich areas on either side, the order of half the fabric thickness (Figure 28(a)), whereas on the other side considerable distortion of the red tow has resulted in a resin rich area below the white tow and above the beige tow. However, it can be deduced from Figure 11 (a) that tows are nested in these locations, and in fact, presenting them as resin rich areas is inaccurate.

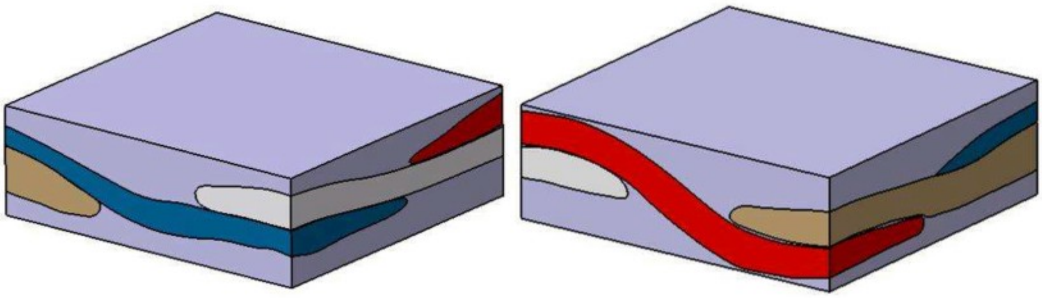

(a) *(b)*

Figure 28: Tow/matrix unit cell: (a) front face; (b) back face.

Note that modelling a single tow from the MicroCT scan results, and repeating it through rotation about the centre of the unit cell results in a poor representation of the tow architecture. This is because each of the individual tow shapes differs, resulting in conflicting dimensions and shapes. Hence, this repetition of a single tow is not recommended.

An alternative to using CATIA in this step would be the use of GEOMAGIC®[1]. This program is designed specifically for altering complex geometries for CAD and FEM purposes.

6.1.4 Fabric assembly and finite element modelling

The assembly was exported into ANSYS Workbench for meshing and analysis. This program was chosen because of its advanced paving ability, which was required in this case to account for the complex geometry.

Four node tetrahedron elements were used to represent all tows and the resin, as shown in Figure 29. This choice of element was based on their ability to construct complex shapes, and the highly irregular geometries of some locations within the fabric structure. In addition, the large number of elements required to represent the structure made it computationally impractical to use higher order elements.

[1] GEOMAGIC®, *Geomagic Inc.*

Symmetrical boundary conditions were applied to all sides. A constant displacement was applied normal to one face of the unit cell, for the purpose of calculating the elastic modulus of the fabric. This was equivalent to a total strain of 1% across the structure. The warp, weft and through-thickness directions were investigated using separate models.

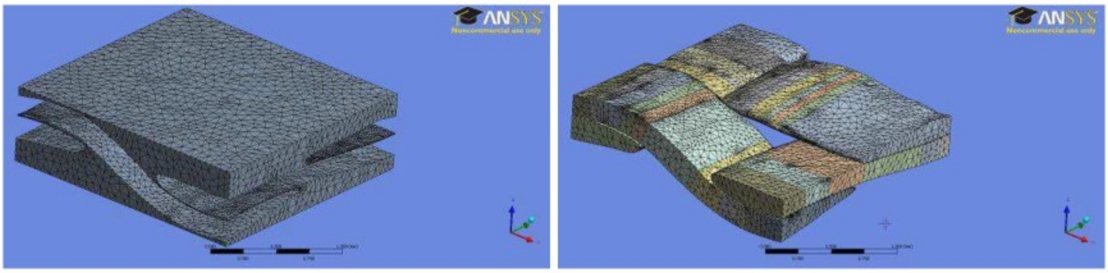

(a) *(b)*

Figure 29: Finite element model of woven fabric; (a) matrix; (b) tows.

In some cases, the use of the paver for meshing has resulted in non-uniform element shapes and dimensions, which may influence results, particularly at stress concentrations. This was accounted for somewhat by specifying gradual element size transitions within the paver options. It is possible that the use of a voxel meshing approach, which has been used previously in the modelling of woven composite tow architectures [12], may reduce this problem.

6.1.5 Material property assignment

The tow properties were evaluated at regular intervals along the fibre axis as shown in Figure 30. The tows were divided into segments of constant orthotropic material property, which were bonded to one another and the matrix using contact. The orientation of the sectioning planes between segments is such that the normal coincides with the fibre direction. In order to minimise the difference in stiffness between neighbouring segments, angular deviation in fibre direction was chosen to be less than 5º. As a result, the locations of the sectioning planes within the tows are non-uniform, which is particularly evident in Figure 30(a).

Each segment was assigned a set of orthotropic material properties. These were calculated based on a rule of mixtures approach [13]. The constituent material properties used for calculation of equivalent properties are summarised in Table 2. Note that the properties of Hexcel F593-18 epoxy resin were used in the place of M36, in order to allow comparison to published material data.

Each tow approximates to a unidirectional composite material. The properties in the fibre direction of the tows were calculated according to Equation 1.

$$E_1 = V_f E_{1f} + (1 - V_f) E_m \tag{1}$$

The transverse tow directions, orthogonal to the fibre direction, were given equal elastic moduli, and were calculated according to Equation 2.

$$E_3 = E_2 = \frac{E_{2f} E_m}{V_f E_m + (1 - V_f) E_{2f}} \tag{2}$$

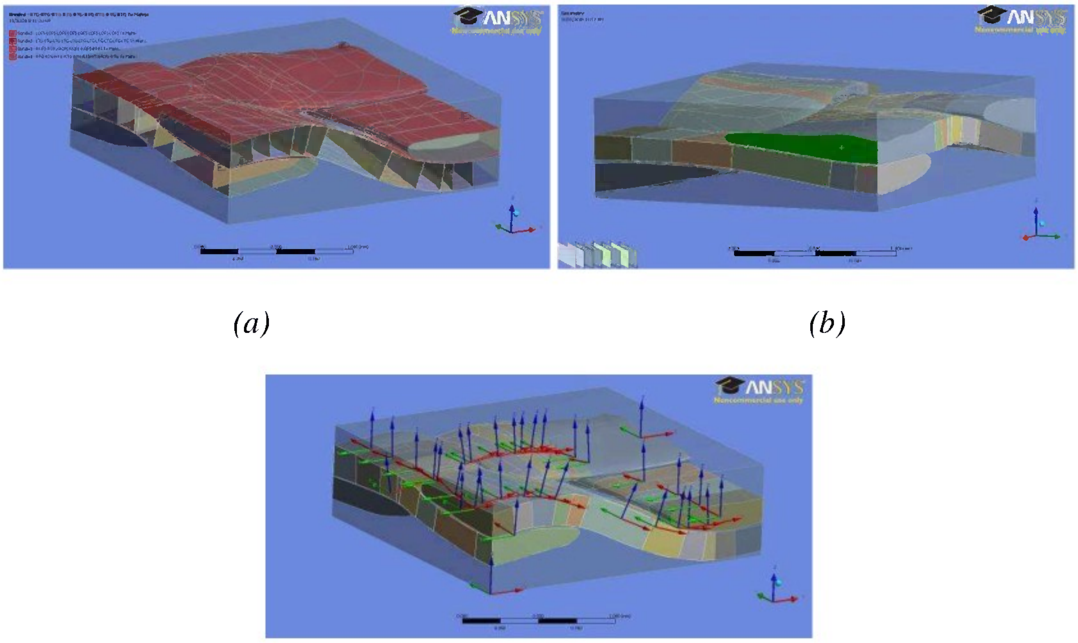

(a) (b) (c)

Figure 30: Segmentation of tows for FEM; (a) tow segmentation; (b) segment area for property calculation shown in green; (c) orientations.

Each tows contains 3000 carbon fibres, having a nominal diameter of 7µm. The average fibre volume fraction of the tow segments can be calculated be comparing the equivalent area of all of the fibres to the area of the tow sectioning planes as shown in Figure 30(b). Since each segment has two sectioning planes, the average is taken as the total tow area, A_{tot}. In the woven fabric structure used in this work, only half of each tow is modelled, hence it is assumed that there are only 1500 carbon fibres in each segment. Accordingly, Equation 3 has been used to calculate the fibre volume fraction, V_f.

$$V_f = \frac{0.057725}{A_{tot}} \quad (3)$$

Table 2: Summary of constituent material properties

Material	Property
T300 Carbon fibre (orthotropic) [14]	$E_1 = 230$ GPa
	$E_2 = E_3 = 15$ GPa
	$G_{12} = G_{23} = G_{31} = 8$ GPa
	$\nu_{12} = 0.38$
	$\nu_{23} = 0.35$
	$\nu_{31} = 0.05$
F593 Epoxy resin (isotropic) [15]	$E = 2.96$ GPa
	$\nu = 0.35$

6.1.6 Results

The elastic modulus of the structure was predicted in the warp, weft and through-thickness directions, based on the force required to sustain a 1% displacement and the outside area of the unit cell. The results are summarised in Table 3.

Table 3: Summary of elastic moduli of fabric.

Direction	Calculated E (GPa)	Experimental E (GPa)
Warp	38.71	56.5 [15]
Weft	43.29	56.5 [15]
Through-thickness	6.62	5.56*
* Unpublished CRC-ACS results		

All of the results differ from those published. In particular, the warp and weft predictions are considerably below the experimental values. This is expected, since the tows from the neighbouring fabrics would generally nest in amongst the tows of the fabric under examination. The fibre volume fraction of the fabric unit cell is lower than expected, which is apparent from the large resin pockets shown in Figure 30. Hence the predicted in-plane elastic moduli are lower than the experimental, due to the more flexible resin being present in the place of the higher stiffness tows. However, this does not account for the higher through-thickness elastic modulus, which may have been contributed to by the dimensional inconsistency of the tows. These observations further reinforce the previously outlined need to consider a more suitable unit cell size, which are discussed further in Section 6.

The equivalent of stress can be seen within the tows as a result of the 1% applied strain in Figure 31. The distribution of stresses is complex in the case of the through-thickness loading, as shown in Figure 31(a). When loaded in the in-plane direction, most of the load is taken by the tows with their fibres oriented in the loading direction, as illustrated in Figure 31(b).

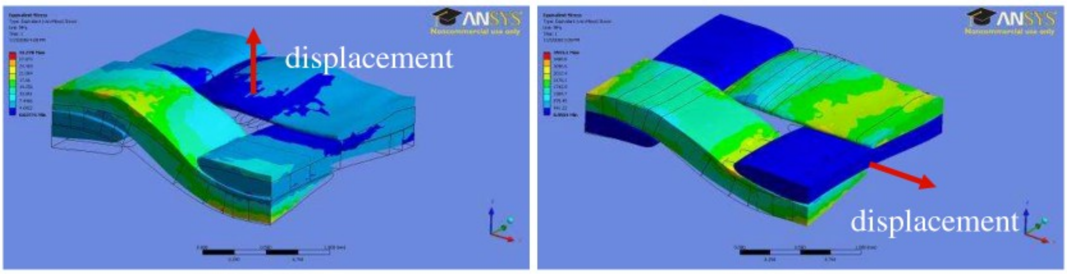

(a) *(b)*

Figure 31: Equivalent of stress plots for tows; (a) through-thickness loading; (b) in-plane loading (weft).

6.2 Voxel FEM approach

6.2.1 Model generation steps

A series of steps is required in order to generate the 3-D fabric models. These must be carried out in the order that follows:

1. Sample manufacture and scanning:
    a. Contrast enhancements must be applied to the tows prior to weaving
    b. Fabric construction and composite consolidation
    c. MicroCT scanning
2. Three-dimensional volume rendering:
    a. Tow volume rendering in tomographic imaging programs (eg: AMIRA®)
    b. Conversion of volumes into a series of cross-sectional images, with each material represented by a single colour.
3. Voxel finite element modelling:
    a. Automated processing of images into a voxel finite element model using purpose written code, ConEnV1.
    b. Assignment of material properties.
    c. Assignment of boundary conditions and tow orientations.
    d. Analysis.

The steps are identical to those described in Section 5 down to 2a, and will not be discussed father. From 2b onwards, the finite element modelling steps are specific to the voxel modelling approach. Note that steps 3c and 3d have not yet been attempted, and may be carried out in the year 2 work package.

6.2.2 Automated meshing and material property assignment

The automated modelling approach, named ConEn V1.0, has been instituted using PYTHON 2.5[1]. Additional sub components of the code required to develop the program include the Python Imaging Library (PIL) and Numpy.

The program works by processing a series of cross-sectional images, from which the 3-D volume is generated. A flow chart detailing simplified steps is shown in Figure 32.

The CT images generated on MGFGI1 were processed using AMIRA. Each individual material, including air, was assigned a single colour. The files were then converted to bitmap images and placed in a single directory for automated conversion into a model.

ConEn begins by examining each of the images. Pixel colour values are loaded into a 3-D array which is representative of the volume. Meanwhile, a nodal coordinate array is generated, which has one more entry in each direction, compared to the number of pixels samples.

[1] PYTHON 2.5, *Python Software Foundation.*

The individual pixel colours are examined. If the pixel colour is not equal to that of the background air, then nodal connectivity is specified to create an element, and the appropriate material is assigned to the element. If the material is air, then nodal connectivity is not assigned. This results in some of the nodes in the nodal coordinate array remaining unused.

All relevant data generated is written out into an MSC.Marc DAT file. This information can be imported into MSC.Mentat, the results of which are shown in Figure 33.

Due to the voxel meshing approach being under development at present, no numerical results are currently available. These will be available following coding of automated orientation and fibre volume fraction assignment algorithms.

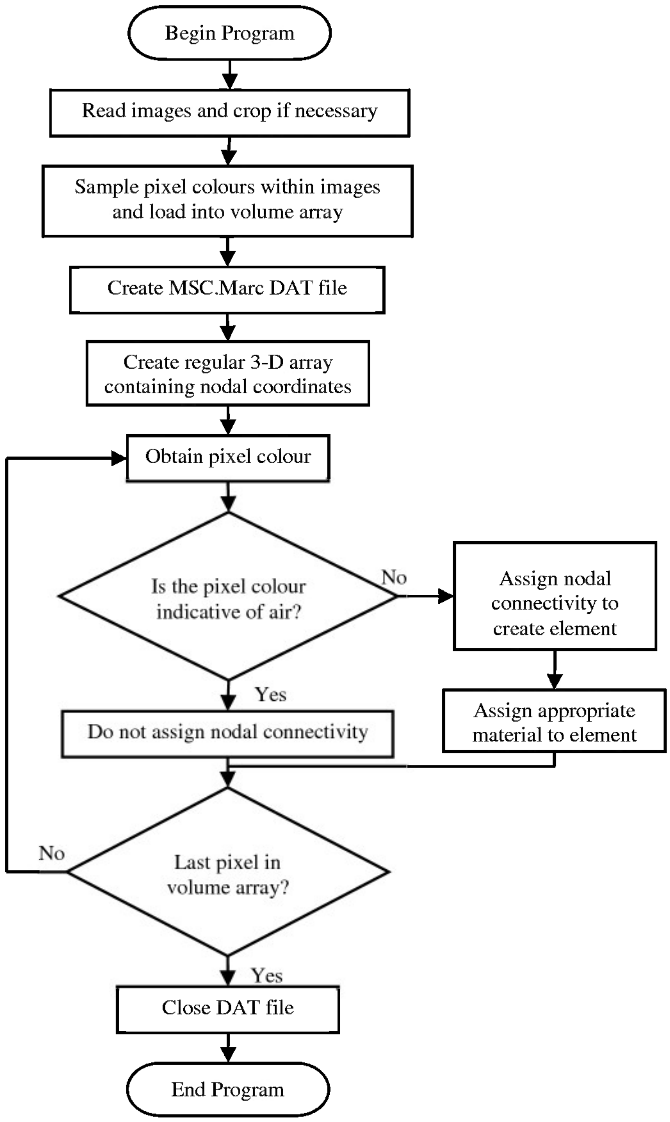

Figure 32: Structure of ConEn V1.0, program to automate voxel model generation.

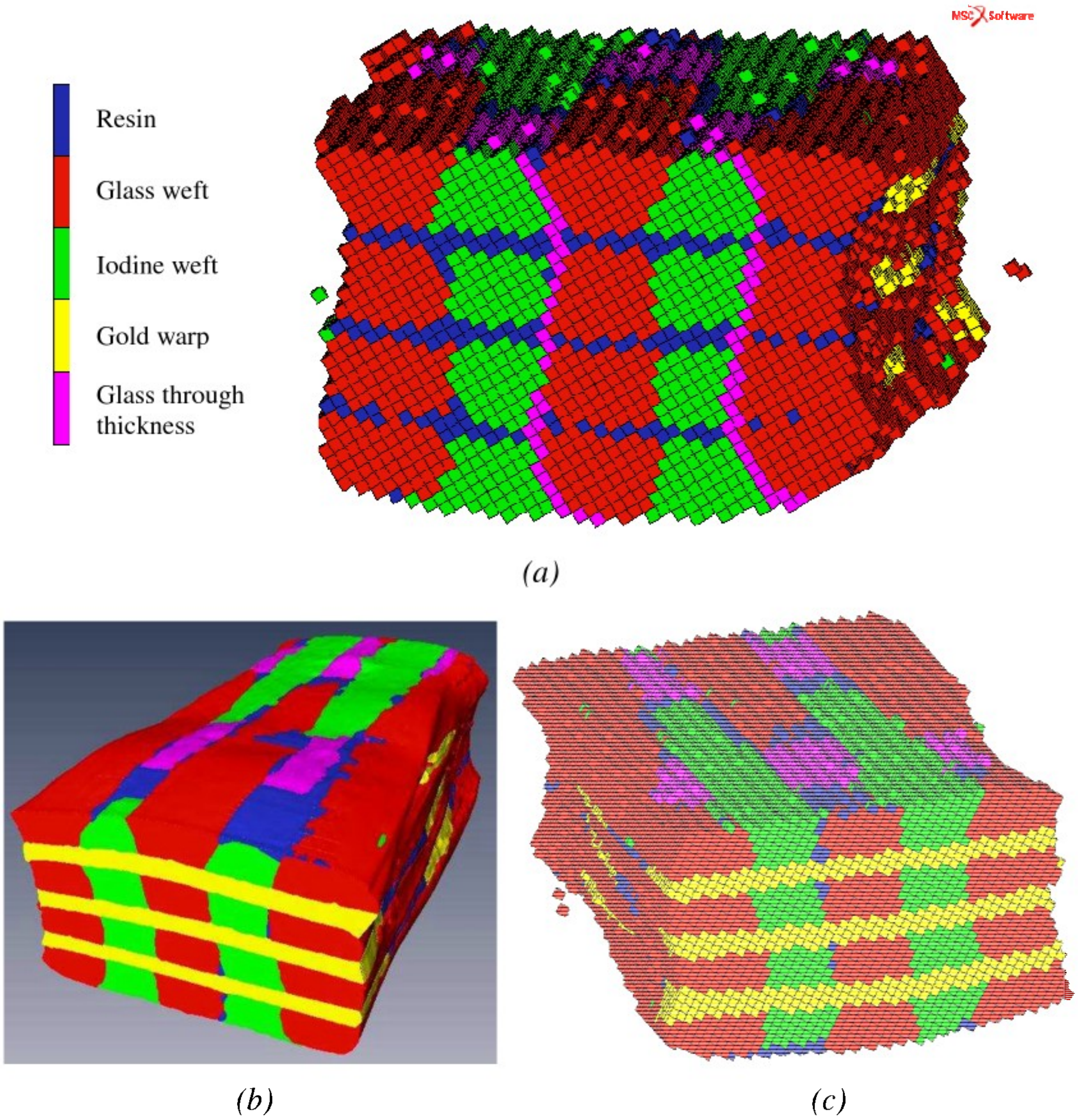

Figure 33: Automated voxel finite element modelling approach; (a) Mesh showing material names; (b) Corresponding volume rendered in AMIRA; (c) Image showing opposite side of mesh to (a).

7 Discussion on tow visualisation methods

The microCT scan results show that all of the contrast enhancement procedures are transferrable from the case of plain woven fabrics, discussed in the previous study, to multi-layer and preform fabrics woven in the custom built loom described in Section 2. Further, the tows used in the previous study were 3K carbon, whereas those reported for this study are 6K carbon; hence, the techniques appear suitable for use on carbon tows of various sizes. Both the Skyscan 1072 and Siemens Inveon microCT scanners are suitable for generating tow visualisations of contrast enhanced fabrics.

It was shown in MI1 (Figure 16) that when two iodine coated tows are placed in contact with one another, the ability to discrimination between the two is diminished, especially if the tows are aligned in the same direction. Hence, if used in this fashion, little benefit is offered from the contrast enhancement methods. This is consistent with previous results [3-4], and is also expected to be the case if two co-aligned glass tows are placed into contact with one another. No such limitation exists between two gold coated tows placed into contact with one another, since the gold interface is still present between the tows, as illustrated in Figure 12.

When a gold tow is placed into contact with an iodine coated tow, the location of the interface between the two is harder to distinguish than in the case of two gold coated tows in contact with one another, as shown in the case of PGI1 and PGI2. The difference is that when there are two gold coated tows in contact with one another, a single gold coated point of contact exists, with untreated carbon present on either side. It is a reasonable assumption that the interface between the two tows is at the centre of the line.

When a gold coated tow is placed into contact with an iodine coated tow, determining the location of the interface between the two tows becomes more difficult. This is due to the gold tow having a coated interface and uncoated interior, and the iodine having a coated interior and exterior. Hence, the interface location cannot be simply assumed to be the centre of the contacting contrast enhanced exteriors, as is the case with the gold coated tows. It is possible that this could result in an error in tow dimension of up to 50 μm, which is an approximation based on the general width of a single gold coating as visualised with the Skyscan 1072.

By interleaving iodine and glass contrast enhancement procedures, in the case of MGFI1, effective contrast enhancement is achieved, as was shown in Figure 21. An additional benefit is achieved by introducing gold as a third type of contrast enhancement, as shown in Figure 22; however, there are instances where the tow coating was too thin, reducing the effectiveness of the contrast enhancement. An alternative method to using different contrast enhancements is to coat of all tows within the laminate with gold, as shown in Figure 20. This also proved to be an effective method; however, folding of the tows may result in confusion as to where the tow interfaces are located, and caution is advised.

Commonly reported tow deformations occur due to the interaction of neighbouring tows during compaction under pressure. This results in distortion of the cross-sectional shapes of the tows. In addition to this deformation, the visualisations of the gold coated tows presented in Figure 19 and Figure 20 reveal that additional deformations occur due to folding of the tows during manufacture. To the Authors' knowledge, no such deformations have been reported previously. It is likely that the folding deformations occur during weaving of the fabric, rather than during infusion of the composite. It is possible that this folding of the tows will cause variations in the local internal fibre directions, hence a variation in the internal tow stiffness. Such an understanding will prove beneficial during modelling of woven composites and should be investigated further.

It was previously reported that the iodine contrast enhancement technique resulted in high void fractions compared to uncoated laminates [3]. The void fractions found in MGFI1 (Figure 21) and MGFGI1 (Figure 22) were similar to that of a regular laminate, without contrast enhancement, even in the locations surrounding the iodine coated tows. Two possible reasons for this improvement were identified. Firstly, the iodine coated tows were of improved flexibility compared to those used previously, as a result of the new preparation method. Secondly, the resin flow to the iodine coated tows is relatively unobstructed, since they were not stacked side-by-side in the laminate, and the permeability and stiffness of the gold coated and glass tows are similar to uncoated laminates as per the void fractions presented in Ref. [3-4]. MG1 and MG2 also had similar void fractions to regular laminates.

In general, the dimension of the laminates which included glass-fibre tows were slightly larger than those of carbon alone, as per the dimensions presented in Table 1. This increase in thickness may be avoided through careful selection of the glass tows.

8 Discussion on FEM

The demonstrated modelling methods allow more reliable representation of tow architectures than the previously used 3-D idealisations. Generation of finite element models from MicroCT image sets has been done previously in the medical field [16] and for non-fibrous metal matrix composites [17], but is new in the field of woven carbon composite research.

There are two main issues that must be addressed. The first of these is the elimination of what is generally considered a "unit cell" architecture; a small idealised arrangement of yarns which can be repeated to describe the entire fabric structure. Unit cells are often used to gain an indication of textile composite properties using planes of symmetry. In reality, no planes of symmetry exist, since the tows have non-uniformly distorted geometries. These perturbations are not only a consideration in the in-plane directions (along the yarns of the same fabric), but also through the thickness (inter-ply interactions such as nesting). Hence, what is generally considered a "unit cell" must be revised under the current modelling strategy. Future research will involve determining a minimum number of warp and weft repetitions, along with plies or layers (through-thickness), to adequately account for geometry variations. This is an even greater consideration when examining three-dimensional preforms.

This issue leads to an additional and potentially even greater drawback; the computing time required to examine the newly defined "unit cell" is much greater than the idealised unit cells. In addition to the FEM incorporating a greater number of yarns, the number of elements per yarn will also increase due to greater complexity of the yarn shape. This is expected to be less of an issue as greater computing resources are developed. Additional simplification and smoothing of the imported tow geometries, discussed in Section 4.2, should allow models with reduced numbers of elements to be constructed whilst maintaining accuracy.

The fibre volume fractions in the conventional finite element model (Section 6.1) were evaluated for each of the tow segments, based on the segment areas normal to the fibre directions. This is once again an approximation. Further deviations in the fibre volume fraction can be considered within each tow segment. In particular, deviations in the through-thickness direction of the tow, particularly at the contact points with other tows, where the fibres are expected to congregate with larger volume fraction. These localised changes to the fibre volume fraction will be considered in future work.

The two modelling processes are very different. The conventional FEM approach is much slower than the voxel FEM approach, although greater control is instituted over the representation of the volume. Typical times required to process the geometry are 1-2 days, which is largely dependent on the proficiency of the user with the software, rather than the computing resource available. Additionally, in the conventional FEM, the elements conform to the boundaries of the tows, often resulting in mesh irregularities due to the use of an automated paver within the ANSYS Workbench pre-processor. In comparison, the automated voxel modelling approach is much faster in developing the model, with typical model development times of 1 to 15 minutes, which is a significant time saving. The voxel method approximates the shape of the tows by applying material properties to a regular mesh. Hence, the irregular element shapes are avoided, unlike the conventional FEM approach. However, the tow boundaries are often represented as jagged, as shown in Figure 33.

Future research will involve further work on the automated voxel meshing approach, currently under development in PYTHON 2.5. This will be used to generate automated approximations to fabrics from microCT scans in the coming years work.

9 Future work

Future work will be conducted according to the timeline shown in Table 4. At the commencement of year 2, work from Qtr.5 will be undertaken. Note that this timeline has been modified with respect to the original timeline:

Table 4: Completed and planned work for research program.

Work package	Qtr from commencement											
	1	2	3	4	5	6	7	8	9	10	11	12
1 Manufacture of 3-D Specimens	■	■	■	■	■	■	■	■				
1.1 Commission loom and tow treatment	■	■										
1.2 Specimens for visualisation trials		■	■									
1.3 Specimens for FEM					■	■						
1.4 Specimens for validation					■	■	■	■				
2 Tow visualisation	■	■	■	■	■	■	■					
2.1 MicroCT		■	■	■	■	■						
3 Imaging processing	■	■	■	■	■	■	■					
3.1 Tomographic image interrogation	■	■	■	■	■	■	■					
3.2 Automatic upload to FEM			■	■	■	■	■					
4 FEA	■	■	■	■	■	■	■	■	■			
4.1 Preliminary FEM to verify feasibility	■	■										
4.2 Model development			■	■	■	■	■	■	■	■	■	
4.3 Stiffness analysis						■	■	■	■	■		
4.4 Strength analysis							■	■	■	■	■	
4.5 Comparison with AFRL results							■	■	■	■	■	
5 Validation						■	■	■	■	■	■	■
5.1 Tension tests						■	■	■				
5.2 Compression Tests						■	■	■				
5.3 Comparison with AFRL results							■	■	■	■	■	
6 Reporting			■	■	■	■	■	■	■	■	■	■

10 Conclusion

The results of year 1 of the research program titled "Tow architecture and mechanical properties of 3-D woven composites (AFOSR/AOARD Grant AOARD 09-4112)" are presented. This year of research had two main objectives, which were to further the contrast enhancement methods developed under the previous grant (AFOSR/AOARD Grant AOARD-07-4003) through application to multi-layer fabric composites, and to complete ground work for finite element modelling of contrast enhanced composites using microCT scan data. Both objectives were completed.

Multi-layer composites were manufactured using a commercial table loom, which was modified for weaving of carbon-fibre composites. Gold, iodine and glass contrast enhancement methods, developed previously, were successfully applied to multi-layer composites. The tows within the composites were visualised using two different methods; (1) coating of the outside of all tows in gold to visualise all tow interfaces; (2) coating of different tows with contrast enhancements of differing density, to identify tows through grayscale colour difference. Both methods produced satisfactory results.

Three dimensional finite element modelling of woven composites, using internal cross sections from microCT scans, was demonstrated to be feasible. Two different approaches to importing composite geometries into finite element pre-processors were developed, for future finite element modelling. The first was conventional finite element modelling, in which the mesh conformed to the tow boundaries. The second was voxel finite element modelling, in which the tow boundary was approximated using elements in a regular arrangement. The voxel finite element modelling is an automated process which significantly reduced modelling times.

References

1. Mouritz, A.P. and Cox, B.N., "A mechanistic interpretation of the comparative in-plane mechanical properties of 3D woven, stitched and pinned composites", *Composites Part A: Applied Science and Manufacturing*, 2010. 41: p. 709-728.
2. Djukic, L., Herszberg, I., Marelli, M. and Hillier, W., "CRC-ACS TM 08021: Enhancement of tow visualisation in 3-D woven composites. AFOSR/AOARD Grant AOARD-07-4003. Final Report", 2008.
3. Djukic, L.P., Herszberg, I., Walsh, W.R., Schoeppner, G.A., Prusty, B.G. and Kelly, D.W., "Contrast enhancement in visualisation of woven composite tow architecture using microCT scanner. Part 1: Fabric coating and resin additives", *Composites Part A: Applied Science and Manufacturing*, 40(5): p.553-565. 2009.
4. Djukic, L.P., Herszberg, I., Walsh, W.R., Schoeppner, G.A. and Prusty, B.G., "Contrast enhancement in visualisation of woven composite architecture using microCT scanner. Part 2: Tow and preform coatings", *Composites Part A: Applied Science and Manufacturing*, 40: p.1870-1879. 2009.
5. Saunders, R.A., C. Lekakou and M.G. Bader, "Compression and microstructure of fibre plain woven cloths in the processing of polymer composites", *Composites Part A: Applied Science and Manufacturing*, 1998. 29(4): p. 443-454.
6. Bogdanovich, A., "Multi-scale modeling, stress and failure analyses of 3-D woven composites", *Journal of Materials Science*, 2006. 41: p. 6547-6590.
7. Bannister, M., I. Herszberg, A. Nicolaidis, F. Coman and K.H. Leong, "The manufacture of glass/epoxy composites with multilayer woven architectures", *Composites Part A: Applied Science and Manufacturing*, 1998. 29(3): p. 293-300.
8. Djukic, L., Herszberg, I. and Marelli, M., "CRC-ACS TM 09078: Development of a weaving loom for multi-layer textile composites. AFOSR/AOARD Grant AOARD 09-4112. Interim Report 1", 2009.
9. Djukic, L. and Herszberg, I., "CRC-ACS TM 09085: Method of rendering images from microCT imagesets. AFOSR/AOARD Grant AOARD 09-4112. Interim Report 2", 2009.
10. Djukic, L. and Herszberg, I., "CRC-ACS TM 09087: Manufacture and microCT scanning of contrast enhanced multi-layer fabrics. AFOSR/AOARD Grant AOARD 09-4112. Interim Report 3", 2009.
11. Djukic, L., Herszberg, I., Wootton, R., Mollenhauer, D., Kelly, D. and Prusty, B., "Characterisation of Woven Composites using Tow Architecture from MicroCT scan" in *13th Australian International Aerospace Congress*, 2009. Melbourne, Vic, Australia.
12. Verpoest, I. and Lomov, S.V., "Virtual textile composites software WiseTex: Integration with micro-mechanical, permeability and structural analysis", *Composites Science and Technology*, 2005, 65(15-16): p. 2563-2574.
13. Daniel, I. and Ishai, O., "Engineering Mechanics of Composite Materials", 1994, Oxford University Press.
14. Torayca, "Technical Datasheet No. CFA-001: T300 Datasheet".
15. Hexcel, "HexPly F593 Product Data", 2005.

16. Lengsfeld, M., Schmitt, J., Alter, P., Kaminsky, J. and Leppek, R., "Comparison of geometry-based and CT voxel-based finite element modelling and experimental validation", *Medical Engineering & Physics*, 1998, 20(7): p. 515-522.

17. Geandier, G., Hazotte, A., Denis, S., Mocellin, A. and Maire, E., "Microstructural analysis of alumina chromium composites by X-ray tomography and 3-D finite element simulation of thermal stresses", *Scripta Materialia*, 2003, 48(8): p. 1219-1224.